applied sciences

MDPI

Article

Dispersion of OH Radicals in Applications Related to Fear-Free Dentistry Using Cold Plasma

Mehrdad Shahmohammadi Beni [1], Wei Han [2,3] and K.N. Yu [1,*]

[1] Department of Physics, City University of Hong Kong, Tat Chee Avenue, Kowloon Tong, Hong Kong, China; mshahmoha2-c@my.cityu.edu.hk

[2] Center of Medical Physics and Technology, Hefei Institutes of Physical Sciences, Chinese Academy of Sciences, Hefei 230031, China; hanw@hfcas.ac.cn

[3] Collaborative Innovation Center of Radiation Medicine of Jiangsu Higher Education Institutions and School for Radiological and Interdisciplinary Sciences (RAD-X), Soochow University, Suzhou 215168, China

* Correspondence: peter.yu@cityu.edu.hk; Tel.: +852-34427182; Fax: +852-34420538

Received: 24 April 2019; Accepted: 20 May 2019; Published: 24 May 2019

Abstract: Cold atmospheric plasmas (CAPs) are being used in applications related to dentistry. Potential benefits include tooth whitening/bleaching, the sterilization of dental cavities, and root canal disinfection. Generated reactive species, such as hydroxyl (OH) radicals, play a critical role in the effectiveness of CAPs in dentistry. In the present work, the mandibular jaw and teeth were modeled. The propagation of CAP plume in ambient air was dynamically tracked using the level set method. The transport and dispersion OH radicals away from the nozzle and towards the teeth under treatment were also tracked. The distributions of concentration of OH radicals over the teeth were obtained for nozzle to tooth distances of 2 and 4 mm. The discharge of the OH radicals out of the nozzle was found to be asymmetrical. Interestingly, depending on the type of tooth treated, the dispersion of OH radicals out of the nozzle could be altered. The present model and obtained results could be useful for advancements towards a fear-free dentistry using CAPs.

Keywords: cold atmospheric plasmas; plasma medicine; dentistry; tooth whitening; fear-free dentistry

1. Introduction

In 1879, the fourth state of matter was unveiled by Sir William Crookes and subsequently in 1929 named "plasma" by Irving Langmuir [1,2]. Moreover, considering the phase transition (e.g., gas to plasma), there was a suggestion that plasmas not be called the fourth state of matter [3]. Plasma research has evolved rapidly and expanded in various areas including environmental, military, agricultural, and biomedical research [4,5]. Cold atmospheric plasmas (CAPs) enhance the generation of reactive species in their flow while the corresponding carrier gases remain at room temperature; this enhances the interaction of the reactive species with the target upon exposure of the latter to CAPs [6]. CAPs were also found useful in surface treatment, material processing, and plasma medicine [7–23]. In the field of medicine/biomedicine, CAPs are found to have significant potential in wound healing [24,25], cancer therapy [26–28], the inactivation of microorganisms [29], and tooth bleaching [21]. In particular, in the dentistry industry, CAPs were found effective against infected dental root canals and could remove microorganisms associated with infection of the root canal [30]. Various studies reported the effective killing of various types of viruses and bacteria by CAPs [31–35]. Considering the favorable characteristics of the CAPs, Stoffels et al. [33,36] were among the pioneers who explored the potential therapeutic use of CAPs in dentistry.

In dentistry, CAP applications were related to tooth whitening/bleaching, sterilization of dental cavities, and root canal disinfection. In a recent review [37], the applications of CAPs in dentistry were reviewed. Interestingly, it was pointed out that CAP treatment of teeth was a new and painless method for the preparation of cavities for restoration, with a rather enhanced longevity, root canal disinfection, and bacterial inactivation. In particular, tooth whitening using CAPs were experimentally studied. For example, Sun et al. [38] deployed a direct current air CAP to enhance tooth whitening. In a separate study, Lee et al. [21] found that a helium CAP jet enhanced tooth bleaching. The combined use of hydrogen peroxide (H_2O_2) with CAPs was found to be three times more effective to enhance tooth bleaching, when compared with the case without CAP. In another study, 40 extracted human molar teeth were treated with carbamide peroxide and additionally exposed to CAP, a plasma arc lamp, and a diode laser, which revealed that exposure to CAPs achieved the most effective tooth bleaching [12]. In addition, Claiborne et al. [39] applied CAP alongside H_2O_2 gel to demonstrate enhanced tooth whitening in 10- and 20-min exposure groups. Interestingly, CAPs were shown to be able to treat irregular surfaces such as dental cavities without the need of mechanical drilling [1]. As CAPs operate at room temperature, they would not exert detrimental effects on the tissues [33]. As regards root canal disinfection, Lu et al. [40] successfully inactivated *Enterococcus faecalis* bacterium in the root canal using a CAP jet device. Shali et al. [41] also examined the effectiveness of CAPs in the disinfection of the tooth root canal. From the progress in the use of CAPs in dentistry, it was hoped that CAPs could lead to fear-free and painless treatments in the near future.

Enhancement in plasma treatment of teeth was attributed to reactive species generated in CAPs, such as hydroxyl (OH) radicals. In the previous work of Pan et al. [42], teeth were exposed to saline solution with an air blow, 5% H_2O_2 gel and saline solution, and a CAP microjet. The authors found that the CAP microjet provided the best tooth whitening, which was due to the OH radicals as revealed using electron spin resonance spectroscopy [42]. In particular, minor enamel surface morphological changes were observed and a rougher surface was formed upon a CAP exposure for 20 min [42]. However, it was anticipated that longer CAP exposures could lead to more substantial morphological changes in the enamel, which might become unacceptable. On the other extreme, underexposures of the teeth to CAPs could jeopardize the efficacy of the treatment.

CAP devices with different designs could generate different distributions of reactive species over treated teeth [43], which could thus affect the treatment effectiveness. To the best of our knowledge, however, there were currently no standardized designs of CAP devices or theoretical models of CAP discharges and distribution of reactive species over teeth for dentistry. Such theoretical models, particularly in a time-dependent (i.e., dynamic) manner, would be critical in the success in applying CAPs to dentistry. Our group previously examined the interaction of CAPs with water medium [44], blood [45], and skin [46] using the finite element method (FEM). More recently, we studied the transport mechanism of OH radicals in CAP discharges and their dispersion and distribution over a skin layer [47], which considered both the diffusion and convection mechanisms in a two-phase flow system (i.e., CAP carrier gas and ambient air). Based on the success of previous models, in the present work, we analyzed the dispersion and distribution of OH radicals generated and distributed by CAPs over treated teeth. The present model could be useful for further development of CAP applications in dentistry, with the view to progress towards fear-free dentistry using CAPs.

2. Materials and Methods

The human mandibular jaw (i.e., the lower jaw) was modeled. Average dimensions of the main parts of the mandibular teeth were taken from previous measurements [48] and are shown in Table 1.

Table 1. Average dimensions of crown and root length of mandibular teeth.

Mandibular Teeth	Crown Length (mm)	Root Length (mm)
Central incisor	8.80	12.6
Lateral incisor	9.40	13.5
Canine	11.0	15.9
First premolar	8.80	14.4
Second premolar	8.20	14.7
First molar	7.70	14.0
Second molar	7.70	13.9
Third molar	7.50	11.8

The modeled mandibular jaw with teeth is shown in Figure 1, in which CAP discharge from a nozzle is also schematically shown. For modeling purposes, the mandibular jaw was placed in a rectangular chamber with the dimensions $90 \times 90 \times 45$ mm^3. The chamber was filled with air and all surfaces were set to be outlets (i.e., exposed to open air). The nozzle was assumed to be filled with helium (He) gas (i.e., the CAP carrier gas). The air in the chamber was assumed to be initially at rest and the plasma carrier gas was injected into the air domain at a specific flow rate Q. The plasma carrier gas (He) was discharged out of the nozzle with a radius of 1 mm and with a flowrate of 1 L/min (Q = 1 L/min) [47]. Following our previous work [47], the propagation of the carrier gas (He) in the air chamber was described using the level set method, since the flow resembled a two-phase flow system. The level set function was

$$\frac{\partial \phi}{\partial t} + \boldsymbol{u} \cdot \nabla \phi = \gamma \nabla \cdot \left(\varepsilon \nabla \phi - \phi(1-\phi) \frac{\nabla \phi}{|\nabla \phi|} \right) \quad (1)$$

where ϕ was the level set variable, $\boldsymbol{u}$ was the velocity field, t was time and γ was introduced for an enhanced numerical stability [49]. The level set function (i.e., Equation (1)) was fully coupled with Equation (2) which described the diffusion and convection of OH radicals:

$$\frac{\partial c_{OH}}{\partial t} + \nabla \cdot (-D_{OH} \nabla c_{OH}) + \boldsymbol{u} \cdot \nabla c_{OH} = S_{OH} + R_{OH} \quad (2)$$

where c_{OH} was the concentration of OH radicals, D was the diffusion coefficient, $\boldsymbol{u}$ was the velocity field, S_{OH} and R_{OH} were the source and reaction terms of the OH radicals [47]. The fluxes of OH radicals were defined in the nozzle to ensure the flow of these species from the nozzle along the axis perpendicular to the target (tooth under CAP treatment). The largest inflow concentration of OH radicals (i.e., at the OH source) was set to be 1 mol/m^3, which simplified the task in obtaining the OH concentrations in a normalized fashion over the target. In addition, variations in concentrations of OH radicals as a result of their reactions were modeled through a decay rate formulation. Interested readers are referred to our previous work [47] for more modeling details and for benchmarking with previous CAP discharge experiments. While OH radicals contributed to the bleaching effect, they might not be the main effectors. Short-lived reactive species in plasma-air-water system were analyzed [50] and different reactive species formed in CAPs were found to be responsible for tooth bleaching. In conventional dental bleaching, H_2O_2 was used (and still is used) as a bleaching agent. It is formed as a result of the recombination of OH radicals and via other reactions. Therefore, the transportation and dispersion of H_2O_2 species were also considered in our computational model in addition to the OH radicals. The diffusion coefficient data for H_2O_2 was taken from the previous work of Tang et al. [51].

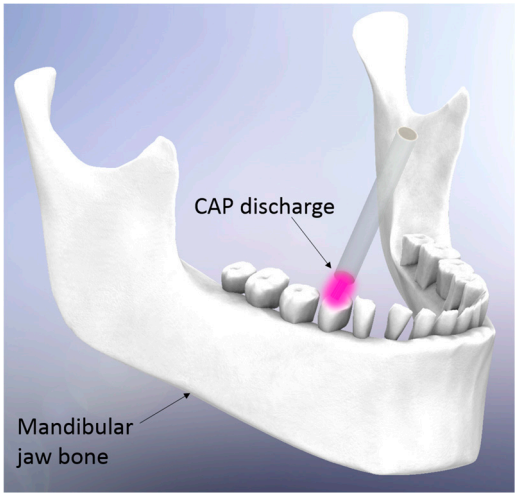

Figure 1. Modeled mandibular jaw with teeth under cold atmospheric plasma (CAP) discharge.

The CAP discharge tube was set to be perpendicular to the tooth under treatment, and the distance between the tube and the tooth was set to be 2 or 4 mm. The eight teeth on one side of the mandibular jaw were, starting from the center, the central and lateral incisor, canine, first and second premolar and first, second and third molar teeth, and eight teeth on the other side, which formed a mirror image of the previous eight teeth. In the present model, the geometry of the incisor and canine teeth were not significantly different from each another, hence, we studied the CAP exposure of six different teeth, namely, canine, first and second premolar and first, and second and third molar teeth. These teeth were numbered from 1 to 6 as shown in Figure 2.

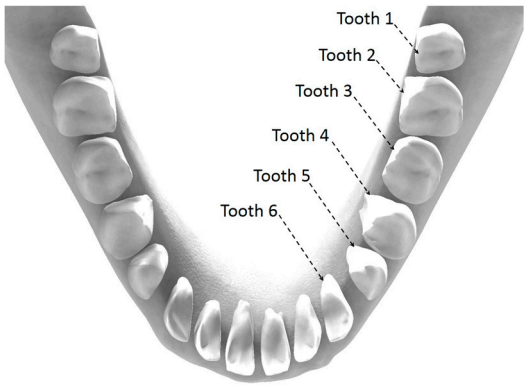

Figure 2. Schematic diagram showing teeth 1 to 6 examined in the present study.

The mandibular jaw bone was not the target of CAP exposures, and was therefore not considered during the computations, which helped improve the computational efficiency (including the total computation time and the required computational resources). The present numerical model was solved in parallel on a computer cluster with Intel Xeon E5-2630 v3 2.40 GHz processors (Intel Corporation, Santa Clara, CA, USA). The system was solved for 10 ms with time steps of 0.01 ms. It would be possible to solve the system using longer time steps; however, it might prevent the model from converging to the final solution effectively. The use of the finest time step was highly recommended, subject to the availability of computational resources.

3. Results and Discussion

During CAP discharge towards a treated tooth, the OH radicals were transported through diffusion and convection from the outlet of the nozzle towards the surface of the tooth. The OH

radicals were distributed over the tooth, which led to a concentration gradient. The spatial variations of the concentration of the OH radicals over teeth 1 to 6 (see Figure 2) for the nozzle to tooth distance of 2 mm were obtained and shown in Figure 3. These snapshots were captured at t = 10 ms (i.e., the final timestep).

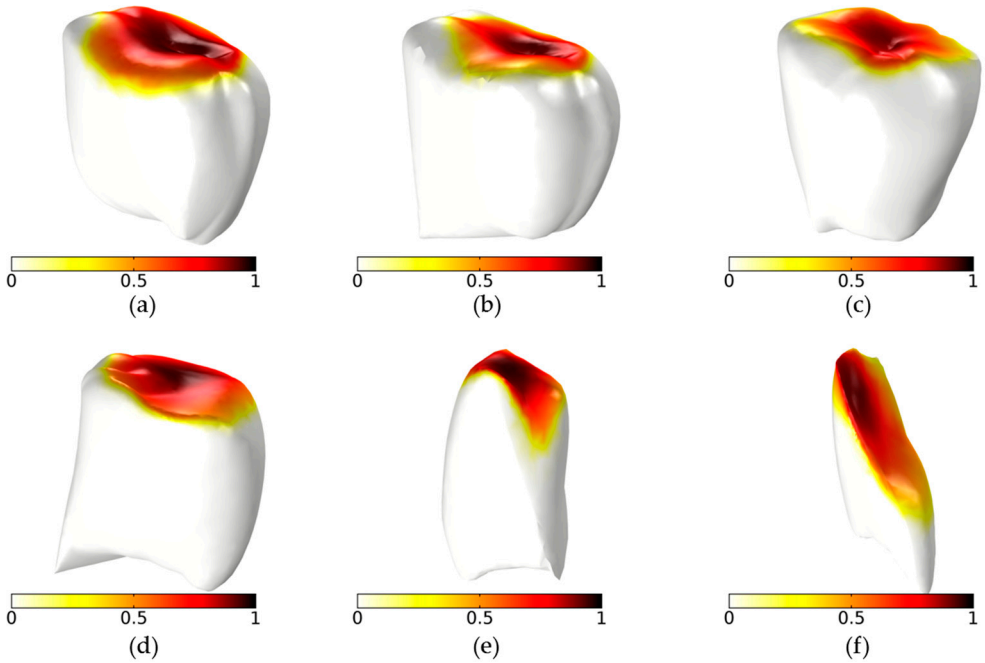

Figure 3. Spatial distribution of OH radicals over tooth (**a**) 1, (**b**) 2, (**c**) 3, (**d**) 4, (**e**) 5 and (**f**) 6 for nozzle to tooth distance of 2 mm. (Note: the scale bar shows the normalized concentration of the OH radicals).

Variations of OH concentrations over the six different exposed teeth for nozzle to tooth distance of 4 mm are shown in Figure 4. These snapshots were captured at t = 10 ms (i.e., the final timestep). To allow easier comparisons, orientations of the teeth were kept the same for both of the nozzle to tooth distances of 2 and 4 mm. Figures 3 and 4 showed that the OH concentration decreased, i.e., fewer OH radicals interacted with the tooth, as the nozzle to tooth distance increased. For longer nozzle to tooth distances, the area on a treated tooth exposed to OH radicals became smaller. Figure 5 also shows that fewer OH radicals could reach the treated tooth for longer nozzle to tooth distances if the speed and time duration were kept constant. Similarly, the variation of H_2O_2 species over the six different exposed teeth for nozzle to tooth distances of 2 and 4 mm are shown in Figures 5 and 6, respectively. The concentrations of H_2O_2 over the teeth decreased with the increasing nozzle to tooth distance, which was explained by the smaller amount of H_2O_2 covering the surfaces of exposed teeth for larger distances. These snapshots were also captured at t = 10 ms (i.e., the final timestep).

The normalized concentration of OH radicals over the tooth started to increase with time upon contact between the CAP plume carrying OH radicals and the tooth. The temporal variations of the normalized concentration of OH radicals averaged over the tooth varied for different teeth, due to their distinct geometries. For the nozzle to tooth distances of 2 and 4 mm, the concentrations of OH radicals started to increase for t > ~1 ms (see Figure 7a) and for t > ~2 ms (see Figure 7b), respectively. The OH radicals needed these onset time durations to travel from the nozzle to the tooth. The temporal variations of H_2O_2 species were similar to those of OH radicals. The H_2O_2 species were distributed over the surface of the exposed tooth and the normalized concentrations increased with time. The OH radicals had a comparatively larger diffusion coefficient compared to the H_2O_2 species [51,52], hence, the temporal variations of normalized concentrations of OH radicals were in general larger than those of the H_2O_2 species. The two main mechanisms for the dispersion of OH species (such as OH and H_2O_2) on different types of teeth were diffusion and convection, both of which were included in

Equation (2). More specifically, the reactive species diffused away from the plasma discharge through diffusion, and they were also carried to different types of teeth by the plasma carrier gas through convection. Figure 7a,b shows the temporal variation of normalized concentrations of OH and H_2O_2 species, respectively, which were averaged over a treated tooth surface. These results quantitatively described the dispersion of reactive species over the surface of the tooth under treatment, which was in turn related to the surface morphology of the tooth. For example, the results for tooth 6 (canine tooth) were significantly different from other molar and premolar teeth, which was attributed to the much sharper tip and smaller size of tooth 6.

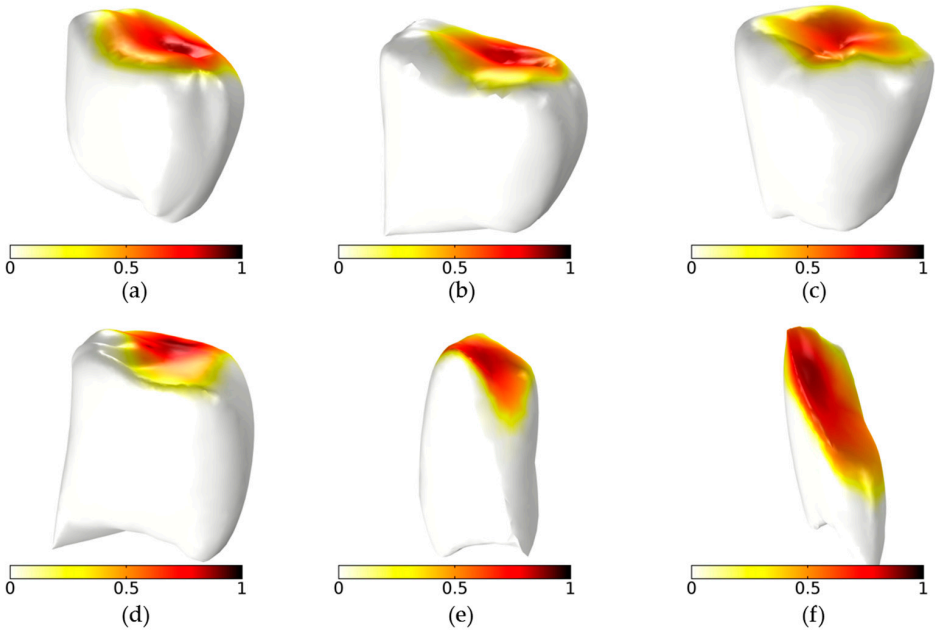

Figure 4. Spatial distribution of OH radicals over tooth (**a**) 1, (**b**) 2, (**c**) 3, (**d**) 4, (**e**) 5 and (**f**) 6 for nozzle to tooth distance of 4 mm. (Note: the scale bar shows the normalized concentration of the OH radicals).

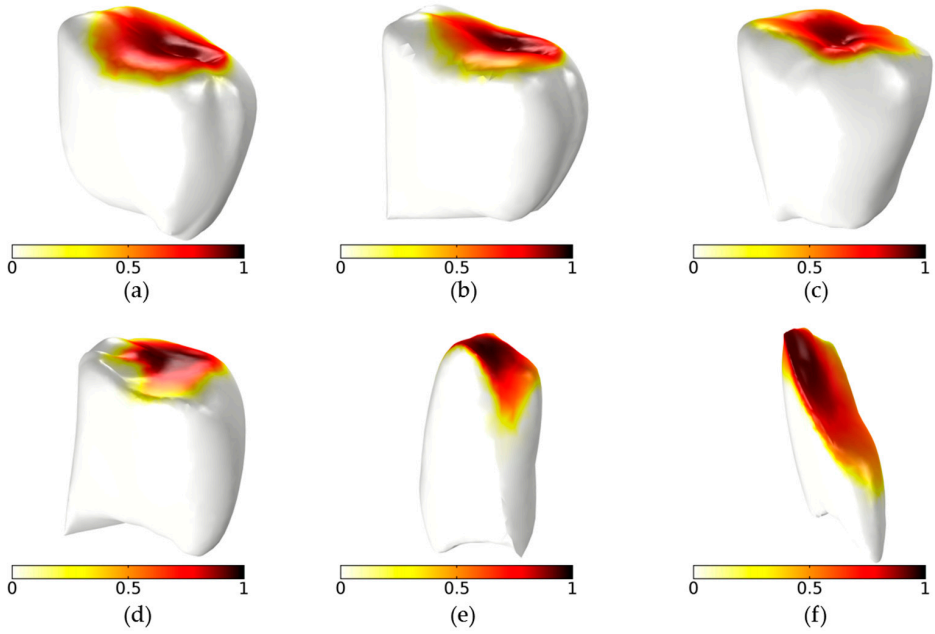

Figure 5. Spatial distribution of H_2O_2 species over tooth (**a**) 1, (**b**) 2, (**c**) 3, (**d**) 4, (**e**) 5 and (**f**) 6 for nozzle to tooth distance of 2 mm. (Note: the scale bar shows the normalized concentration of the H_2O_2 species).

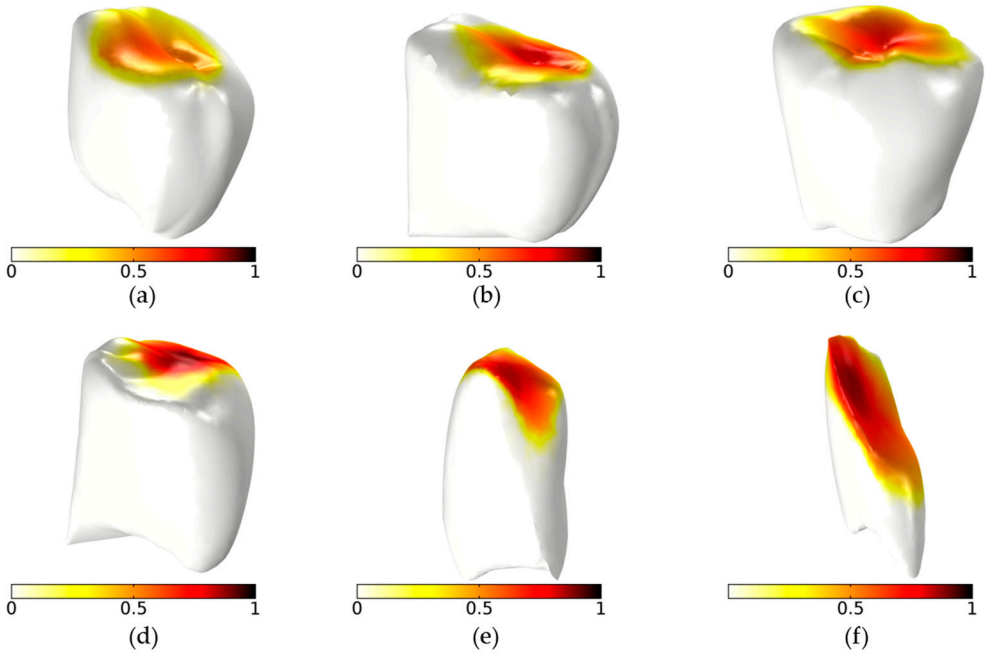

Figure 6. Spatial distribution of H_2O_2 species over tooth (**a**) 1, (**b**) 2, (**c**) 3, (**d**) 4, (**e**) 5 and (**f**) 6 for nozzle to tooth distance of 4 mm. (Note: the scale bar shows the normalized concentration of the H_2O_2 species).

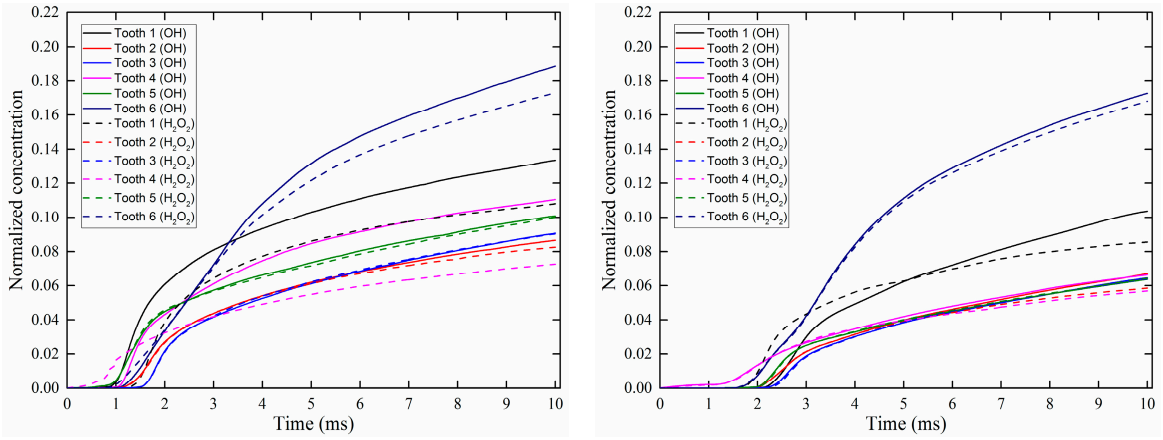

Figure 7. Temporal variations of normalized concentration of OH radicals and H_2O_2 species averaged over a treated tooth for nozzle to tooth distance of (**a**) 2 and (**b**) 4 mm.

To ascertain the steady-state in the studied system, the speed at 1 mm below the center of the nozzle was separately determined for all six teeth. The temporal variations of speeds at 1 mm below the center of the nozzle are shown in Figure 8a,b for 2 and 4 mm nozzle to tooth distances, respectively. The speed started to increase with time up to 1 ms, and became constant for the longer exposure time, which demonstrated the steady-state in the studied system. Moreover, the determined speeds varied for different treated teeth. Following the contact between the carrier gas and the tooth, the flow would get distorted and a velocity field would be generated (i.e., eddies would be formed) around the tooth. The distribution of this velocity field in three-dimensional (3D) space depended on the geometry of the treated tooth (or in other words how the flow was distorted), and led to variations in the speed (the magnitude of velocity in 3D space) at a point from the tooth.

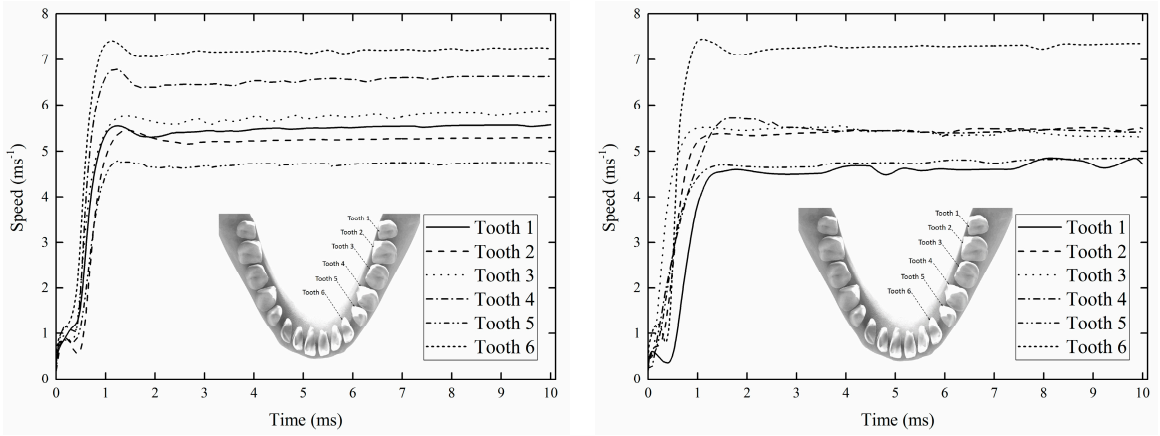

Figure 8. Temporal variations of speed at 1 mm below the center of the nozzle for nozzle to tooth distance of (**a**) 2 and (**b**) 4 mm.

Figure 9a,b shows variations of normalized concentrations of OH radicals at 1 mm below the center of the nozzle for all six teeth at nozzle to tooth distances of 2 and 4 mm, respectively. The normalized concentrations started to increase rapidly up to about 1 in ~1 ms, beyond which the steady-state condition was achieved. Small variations for different teeth were noticed, which were attributed to the distortion of the flow and variations in the velocity field around different teeth under CAP treatment. Such variations were governed by the convection of the OH radicals, since the velocity field determined the dispersion and distribution of these species, which was mathematically shown in Equation (2), where the velocity field $\boldsymbol{u}$ was present. The results in Figure 9 imply that the movement of the OH radicals reached the steady-state as well.

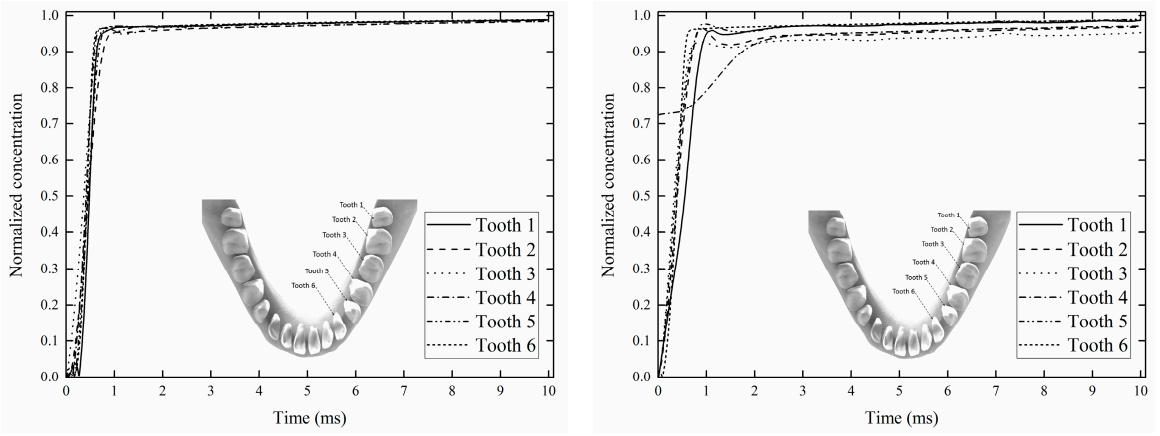

Figure 9. Variations of normalized concentration of OH radicals at 1 mm below the center of the nozzle for nozzle to tooth distances of (**a**) 2 and (**b**) 4 mm.

Figure 10 shows the normalized concentrations of the OH radicals around the four sides at 1 mm below the nozzle, which were obtained for the nozzle to tooth distance of 2 mm. The results revealed anisotropy of dispersion and distribution of OH radicals underneath the nozzle and variations of the dispersion for different teeth. Interestingly, the normalized concentrations away from the center of the nozzle were lower than 1, which meant that most discharged OH radicals were concentrated at the center of the CAP plume. This feature was particularly useful considering that very narrow regions in teeth were often treated in dentistry. For t < ~1 ms, the normalized concentrations significantly varied

with time. In contrast, after the system reached the steady-state (i.e., t > ~1 ms), temporal variations in the normalized concentrations of OH radicals became negligible.

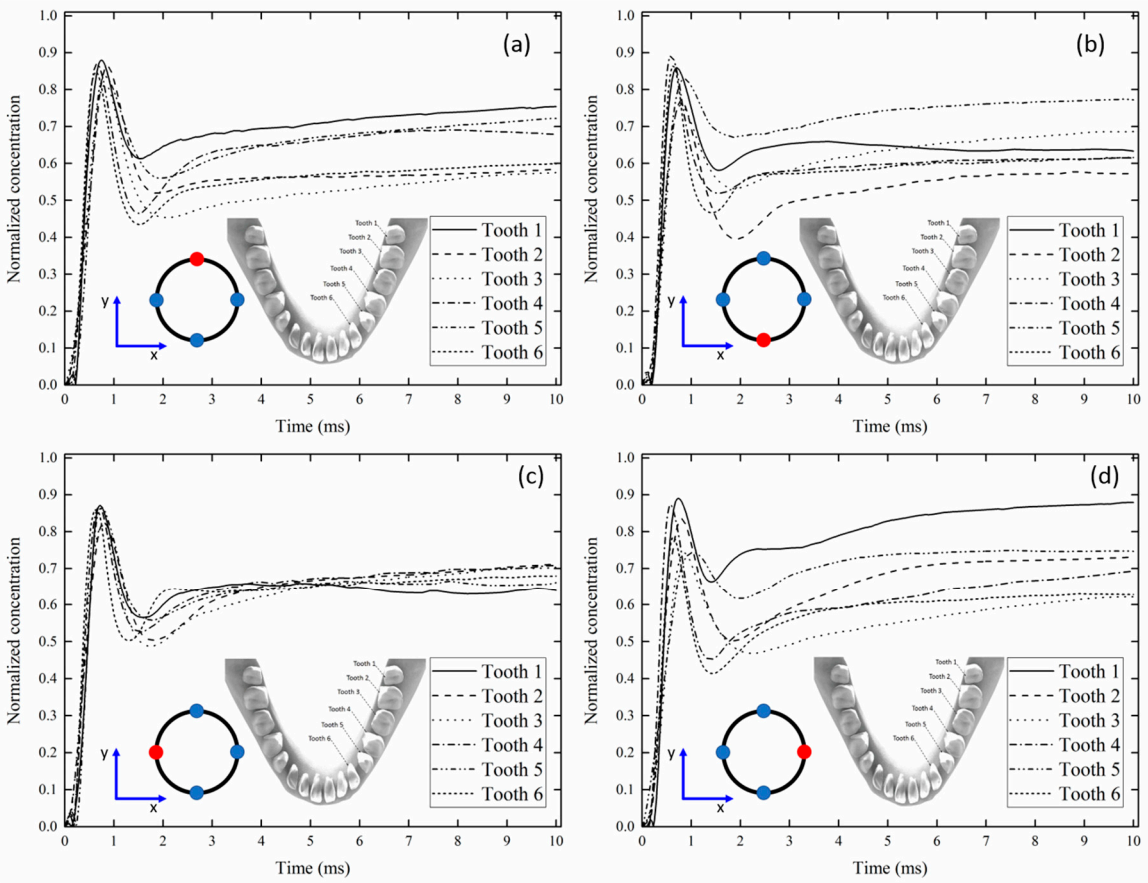

Figure 10. Variations of normalized concentrations of OH radicals at 1 mm below the nozzle at 1 mm (**a**) above, (**b**) below, (**c**) left, and (**d**) right of the center of the nozzle (from bird's eye view), for nozzle to tooth distance of 2 mm. (Inset: red dot indicates the location where the normalized concentration of OH was measured).

Similarly, Figure 11 shows the normalized concentrations of the OH radicals around the four sides at 1 mm below the nozzle, which were obtained for the nozzle to tooth distance of 4 mm. Again, temporal variations in the normalized concentrations of OH radicals were negligible for t > ~1 ms. Variations of normalized concentrations of OH radicals around the four sides of the nozzle were more considerable for the nozzle to tooth distance of 4 mm, which were attributed to the dispersion of OH radicals in the surrounding air before interacting with the tooth. For the longer nozzle to tooth distance of 4 mm, the OH radicals traveled longer distances to reach the tooth, which allowed some OH radicals to travel laterally away from the center of the flow through diffusion (i.e., $\nabla\cdot(-D_{OH}\nabla c_{OH})$ term in Equation (2)). Solving the present model in 3D space was in fact required due to anisotropic dispersion of the OH radicals.

In summary, Figures 10 and 11 highlighted the asymmetrical and sophisticated nature of dispersion and discharge of OH radicals out of the nozzle, which depended on the nozzle to tooth distance, as well as the type of tooth under treatment. Using the present model, the different geometries of nozzles and discharge tubes could be modeled with a view to achieving the best output distribution of reactive species according to the treatment requirements. Information regarding the distribution of reactive species could also be obtained to provide quantitative comparisons among different designs of CAP devices in dentistry.

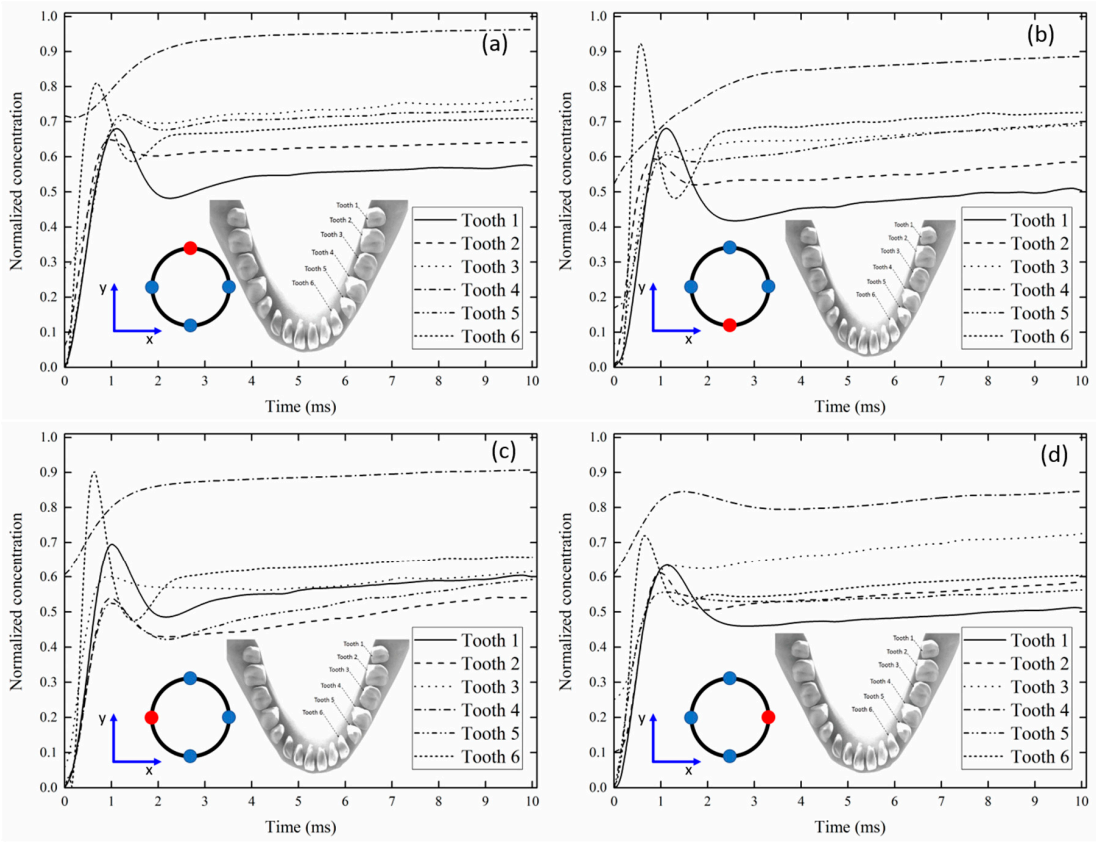

Figure 11. Variations of normalized concentrations of OH radicals at 1 mm below the nozzle at 1 mm (**a**) above, (**b**) below, (**c**) left, and (**d**) right of the center of the nozzle (from bird's eye view), for nozzle to tooth distance of 4 mm. (Inset: red dot indicates the location where the normalized concentration of OH was measured).

4. Conclusions

In the present work, a model was built for CAP discharges on teeth for dentistry applications for the first time. The model considered the CAP carrier gas and the ambient air through a two-phase flow model, and took into account the transport of OH radicals and H_2O_2 species involving diffusion and convection. The developed model determined the distributions of OH radicals and H_2O_2 species over six different chosen teeth. Different nozzle to tooth distances of 2 and 4 mm were examined and the obtained results were compared. The normalized concentration of OH radicals and H_2O_2 species over a treated tooth decreased with the increasing nozzle to tooth distance. The distribution of OH radicals out of the nozzle was found to be asymmetrical. The dispersion of OH radicals out of the nozzle varied according to the type of treated tooth. The dispersion of the reactive species became more significant for shorter distances between the nozzle and the tooth, which led to the coverage of a larger surface area of the tooth during plasma treatment. As such, the treatment could be more efficient. The developed model and the obtained results could be useful for working towards a fear-free dentistry using CAPs.

Author Contributions: Conceptualization, M.S.B.; methodology, M.S.B.; formal analysis, M.S.B., K.N.Y.; investigation, M.S.B.; resources, M.S.B., W.H., K.N.Y.; writing—original draft preparation, M.S.B.; writing—review and editing, W.H., K.N.Y.; visualization, M.S.B.; supervision, K.N.Y.; project administration, K.N.Y.; funding acquisition, W.H., K.N.Y.

Funding: This work was funded by National Natural Science Foundation of China (Nos. U1632145, 81573093 and 81227902), a project funded by the Priority Academic Program Development of Jiangsu Higher Education Institutions (PAPD) and Jiangsu Provincial Key Laboratory of Radiation Medicine and Protection, China Postdoctoral Science Foundation (No. 2016M592584).

Acknowledgments: We acknowledge the support of the Neutron computer cluster from the Department of Physics, City University of Hong Kong, for the computational work involved in this paper.

Conflicts of Interest: The authors declare no conflict of interest.

References

1. Kumar, S.C.; Sarada, P.; Reddy, S.C.; Reddy, S.M.; DSV, N. Plasma torch toothbrush a new insight in fear free dentisry. *J. Clin. Diagn. Res.* **2014**, *8*. [CrossRef]
2. Cha, S.; Park, Y.S. Plasma in dentistry. *Clin. Plasma Med.* **2014**, *2*, 4–10. [CrossRef] [PubMed]
3. Burm, K.T. Plasma: The fourth state of matter. *Plasma Chem. Plasma Process.* **2012**, *32*, 401–407. [CrossRef]
4. Heinlin, J.; Isbary, G.; Stolz, W.; Morfill, G.; Landthaler, M.; Shimizu, T.; Steffes, B.; Nosenko, T.; Zimmermann, J.L.; Karrer, S. Plasma applications in medicine with a special focus on dermatology. *J. Eur. Acad. Dermatol. Venereol.* **2011**, *25*, 1–11. [CrossRef]
5. Heinlin, J.; Morfill, G.; Landthaler, M.; Stolz, W.; Isbary, G.; Zimmermann, J.L.; Shimizu, T.; Karrer, S. Plasma medicine: Possible applications in dermatology. *J. Dtsch. Dermatol. Ges.* **2010**, *8*, 968–976. [CrossRef] [PubMed]
6. Pan, J.; Sun, K.; Liang, Y.; Sun, P.; Yang, X.; Wang, J.; Zhang, J.; Zhu, W.; Fang, J.; Becker, K.H. Cold plasma therapy of a tooth root canal infected with Enterococcus faecalis biofilms in vitro. *J. Endod.* **2013**, *39*, 105–110. [CrossRef]
7. Lu, X.; Naidis, G.V.; Laroussi, M.; Reuter, S.; Graves, D.B.; Ostrikov, K. Reactive species in non-equilibrium atmospheric-pressure plasmas: Generation, transport, and biological effects. *Phys. Rep.* **2016**, *630*. [CrossRef]
8. Lu, X.; Naidis, G.V.; Laroussi, M.; Ostrikov, K. Guided ionization waves: Theory and experiments. *Phys. Rep.* **2014**, *540*, 123–166. [CrossRef]
9. Graves, D.B. Low temperature plasma biomedicine: A tutorial review. *Phys. Plasmas* **2014**, *21*, 080901. [CrossRef]
10. Murakami, T.; Niemi, K.; Gans, T.; O'Connell, D.; Graham, W.G. Chemical kinetics and reactive species in atmospheric pressure helium–oxygen plasmas with humid-air impurities. *Plasma Sources Sci. Technol.* **2012**, *22*, 015003. [CrossRef]
11. Ji, L.; Bi, Z.; Niu, J.; Fan, H.; Liu, D. Atmospheric-pressure microplasmas with high current density confined inside helium-filled hollow-core fibers. *Appl. Phys. Lett.* **2013**, *102*, 184105. [CrossRef]
12. Nam, S.H.; Lee, H.W.; Cho, S.H.; Lee, J.K.; Jeon, Y.C.; Kim, G.C. High-efficiency tooth bleaching using non-thermal atmospheric pressure plasma with low concentration of hydrogen peroxide. *J. Appl. Oral Sci.* **2013**, *21*, 265–270. [CrossRef] [PubMed]
13. Foest, R.; Kindel, E.; Lange, H.; Ohl, A.; Stieber, M.; Weltmann, K.D. RF capillary jet-a tool for localized surface treatment. *Contrib. Plasma Phys.* **2007**, *47*, 119–128. [CrossRef]
14. Reuter, R.; Rügner, K.; Ellerweg, D.; de los Arcos, T.; von Keudell, A.; Benedikt, J. The role of oxygen and surface reactions in the deposition of silicon oxide like films from HMDSO at atmospheric pressure. *Plasma Process. Polym.* **2012**, *9*, 1116–1124. [CrossRef]
15. Murakami, T.; Niemi, K.; Gans, T.; O'Connell, D.; Graham, W.G. Afterglow chemistry of atmospheric-pressure helium–oxygen plasmas with humid air impurity. *Plasma Sources Sci. Technol.* **2014**, *23*, 025005. [CrossRef]
16. Naidis, G.V. Production of active species in cold helium–air plasma jets. *Plasma Sources Sci. Technol.* **2014**, *23*, 065014. [CrossRef]
17. Winter, J.; Brandenburg, R.; Weltmann, K.D. Atmospheric pressure plasma jets: An overview of devices and new directions. *Plasma Sources Sci. Technol.* **2015**, *24*, 064001. [CrossRef]
18. Flynn, P.B.; Busetti, A.; Wielogorska, E.; Chevallier, O.P.; Elliott, C.T.; Laverty, G.; Gorman, S.P.; Graham, W.G.; Gilmore, B.F. Non-thermal plasma exposure rapidly attenuates bacterial AHL-dependent quorum sensing and virulence. *Sci. Rep.* **2016**, *6*, 26320. [CrossRef] [PubMed]
19. Ikawa, S.; Kitano, K.; Hamaguchi, S. Effects of pH on bacterial inactivation in aqueous solutions due to low-temperature atmospheric pressure plasma application. *Plasma Process. Polym.* **2010**, *7*, 33–42. [CrossRef]
20. Laroussi, M. Low temperature plasma-based sterilization: Overview and state-of-the-art. *Plasma Process. Polym.* **2005**, *2*, 391–400. [CrossRef]
21. Lee, H.W.; Kim, G.J.; Kim, J.M.; Park, J.K.; Lee, J.K.; Kim, G.C. Tooth bleaching with nonthermal atmospheric pressure plasma. *J. Endod.* **2009**, *35*, 587–591. [CrossRef]

22. Laroussi, M. From killing bacteria to destroying cancer cells: 20 years of plasma medicine. *Plasma Process. Polym.* **2014**, *11*, 1138–1141. [CrossRef]
23. Kaushik, N.K.; Kim, Y.H.; Han, Y.G.; Choi, E.H. Effect of jet plasma on T98G human brain cancer cells. *Curr. Appl. Phys.* **2013**, *13*, 176–180. [CrossRef]
24. Isbary, G.; Morfill, G.; Schmidt, H.U.; Georgi, M.; Ramrath, K.; Heinlin, J.; Karrer, S.; Landthaler, M.; Shimizu, T.; Steffes, B.; et al. A first prospective randomized controlled trial to decrease bacterial load using cold atmospheric argon plasma on chronic wounds in patients. *Br. J. Dermatol.* **2010**, *163*, 78–82. [CrossRef]
25. Arndt, S.; Unger, P.; Wacker, E.; Shimizu, T.; Heinlin, J.; Li, Y.F.; Thomas, H.M.; Morfill, G.E.; Zimmermann, J.L.; Bosserhoff, A.K.; et al. Cold atmospheric plasma (CAP) changes gene expression of key molecules of the wound healing machinery and improves wound healing in vitro and in vivo. *PLoS ONE* **2013**, *8*, e79325. [CrossRef]
26. Cheng, X.; Murphy, W.; Recek, N.; Yan, D.; Cvelbar, U.; Vesel, A.; Mozetič, M.; Canady, J.; Keidar, M.; Sherman, J.H. Synergistic effect of gold nanoparticles and cold plasma on glioblastoma cancer therapy. *J. Phys. D Appl. Phys.* **2014**, *47*, 335402. [CrossRef]
27. Cheng, X.; Sherman, J.; Murphy, W.; Ratovitski, E.; Canady, J.; Keidar, M. The Effect of Tuning Cold Plasma Composition on Glioblastoma Cell Viability. *PLoS ONE* **2014**, *9*, e98652. [CrossRef]
28. Yan, D.; Talbot, A.; Nourmohammadi, N.; Cheng, X.; Canady, J.; Sherman, J.; Keidar, M. Principles of using cold atmospheric plasma stimulated media for cancer treatment. *Sci. Rep.* **2015**, *5*, 18339. [CrossRef]
29. Noriega, E.; Shama, G.; Laca, A.; Díaz, M.; Kong, M.G. Cold atmospheric gas plasma disinfection of chicken meat and chicken skin contaminated with Listeria innocua. *Food Microbiol.* **2011**, *28*, 1293–1300. [CrossRef]
30. Jiang, C.; Chen, M.T.; Gorur, A.; Schaudinn, C.; Jaramillo, D.E.; Costerton, J.W.; Sedghizadeh, P.P.; Vernier, P.T.; Gundersen, M.A. Nanosecond pulsed plasma dental probe. *Plasma Process. Polym.* **2009**, *6*, 479–483. [CrossRef]
31. Kuo, S.P.; Bivolaru, D.; Williams, S.; Carter, C.D. A microwave-augmented plasma torch module. *Plasma Sources Sci. Technol.* **2006**, *15*, 266. [CrossRef]
32. Tang, Y.Z.; Lu, X.P.; Laroussi, M.; Dobbs, F.C. Sublethal and killing effects of atmospheric-pressure, nonthermal plasma on eukaryotic microalgae in aqueous media. *Plasma Process. Polym.* **2008**, *5*, 552–558. [CrossRef]
33. Sladek, R.E.; Stoffels, E.; Walraven, R.; Tielbeek, P.J.; Koolhoven, R.A. Plasma treatment of dental cavities: A feasibility study. *IEEE Trans. Plasma Sci.* **2004**, *32*, 1540–1543. [CrossRef]
34. Stoffels, E.; Kieft, I.E.; Sladek, R.E.; Van den Bedem, L.J.; Van der Laan, E.P.; Steinbuch, M. Plasma needle for in vivo medical treatment: Recent developments and perspectives. *Plasma Sources Sci. Technol.* **2006**, *15*, S169. [CrossRef]
35. Sladek, R.E.; Filoche, S.K.; Sissons, C.H.; Stoffels, E. Treatment of Streptococcus mutans biofilms with a nonthermal atmospheric plasma. *Lett. Appl. Microbiol.* **2007**, *45*, 318–323. [CrossRef]
36. Stoffels, E.; Flikweert, A.J.; Stoffels, W.W.; Kroesen, G.M. Plasma needle: A non-destructive atmospheric plasma source for fine surface treatment of (bio) materials. *Plasma Sources Sci. Technol.* **2002**, *11*, 383. [CrossRef]
37. Arora, V.; Nikhil, V.; Suri, N.K.; Arora, P. Cold atmospheric plasma (CAP) in dentistry. *Dentistry* **2014**, *4*, 1. [CrossRef]
38. Sun, P.; Pan, J.; Tian, Y.; Bai, N.; Wu, H.; Wang, L.; Yu, C.; Zhang, J.; Zhu, W.; Becker, K.H.; et al. Tooth whitening with hydrogen peroxide assisted by a direct-current cold atmospheric-pressure air plasma microjet. *IEEE Trans. Plasma Sci.* **2010**, *38*, 1892–1896.
39. Claiborne, D.; McCombs, G.; Lemaster, M.; Akman, M.A.; Laroussi, M. Low-temperature atmospheric pressure plasma enhanced tooth whitening: The next-generation technology. *Int. J. Dent. Hyg.* **2014**, *12*, 108–114. [CrossRef]
40. Lu, X.; Cao, Y.; Yang, P.; Xiong, Q.; Xiong, Z.; Xian, Y.; Pan, Y. An RC plasma device for sterilization of root canal of teeth. *IEEE Trans. Plasma Sci.* **2009**, *37*, 668–673.
41. Shali, P.; Asadi, P.; Ashari, M.A.; Shokri, B. Cold atmospheric pressure plasma jet for tooth root canal disinfection. In Proceedings of the IEEE International Conference on Plasma Sciences (ICOPS), Antalya, Turkey, 24–28 May 2015.
42. Pan, J.; Sun, P.; Tian, Y.; Zhou, H.; Wu, H.; Bai, N.; Liu, F.; Zhu, W.; Zhang, J.; Becker, K.H.; et al. A novel method of tooth whitening using cold plasma microjet driven by direct current in atmospheric-pressure air. *IEEE Trans. Plasma Sci.* **2010**, *38*, 3143–3151. [CrossRef]

43. Yue, Y.; Pei, X.; Lu, X. Comparison on the absolute concentrations of hydroxyl and atomic oxygen generated by five different nonequilibrium atmospheric-pressure plasma jets. *IEEE Trans. Radiat. Plasma Med. Sci.* **2017**, *1*, 541–549. [CrossRef]
44. Shahmohammadi Beni, M.; Yu, K.N. Computational fluid dynamics analysis of cold plasma carrier gas injected into a fluid using level set method. *Biointerphases* **2015**, *10*, 041003. [CrossRef]
45. Shahmohammadi Beni, M.; Yu, K.N. Computational Fluid Dynamics Analysis of Cold Plasma Plume Mixing with Blood Using Level Set Method Coupled with Heat Transfer. *Appl. Sci.* **2017**, *7*, 578. [CrossRef]
46. Shahmohammadi Beni, M.; Yu, K.N. Safeguarding against inactivation temperatures during plasma treatment of skin: Multiphysics model and phase field method. *Math. Comput. Appl.* **2017**, *22*, 24. [CrossRef]
47. Shahmohammadi Beni, M.; Han, W.; Yu, K.N. Modeling OH transport phenomena in cold plasma discharges using level set method. *Plasma Sci. Technol.* **2019**, *21*, 055403. [CrossRef]
48. Scheid, R.C. *Woelfel's Dental Anatomy*; Lippincott Williams & Wilkins: Philadelphia, PA, USA, 2012.
49. Shahmohammadi Beni, M.; Zhao, J.; Yu, K.N. Investigation of droplet behaviors for spray cooling using level set method. *Ann. Nucl. Energy* **2018**, *113*, 162–170. [CrossRef]
50. Gorbanev, Y.; Privat-Maldonado, A.; Bogaerts, A. Analysis of Short-Lived Reactive Species in Plasma–Air–Water Systems: The Dos and the Do Nots. *Anal. Chem.* **2018**, *90*, 13151–13158. [CrossRef] [PubMed]
51. Tang, M.J.; Cox, R.A.; Kalberer, M. Compilation and evaluation of gas phase diffusion coefficients of reactive trace gases in the atmosphere: Volume 1. Inorganic compounds. *Atmos. Chem. Phys.* **2014**, *14*, 9233–9247. [CrossRef]
52. Liu, Y.; Ivanov, A.V.; Molina, M.J. Temperature dependence of OH diffusion in air and He. *Geophys. Res. Lett.* **2009**, *36*, L03816. [CrossRef]